



## Research article

# Follicular fluid aids cell adhesion, spreading in an age independent manner and shows an age-dependent effect on DNA damage in fallopian tube epithelial cells

Amrita Salvi <sup>a</sup>, Wenping Li <sup>b</sup>, Shweta S. Dipali <sup>c</sup>, Stephanie M. Cologna <sup>b</sup>, Mary Ellen Pavone <sup>c</sup>, Francesca E. Duncan <sup>c</sup>, Joanna E. Burdette <sup>a,\*,1</sup>

<sup>a</sup> Department of Pharmaceutical Sciences, College of Pharmacy, University of Illinois Chicago, Chicago, IL, 60607, USA

<sup>b</sup> Department of Chemistry, University of Illinois Chicago, Chicago, IL, 60607, USA

<sup>c</sup> Department of Obstetrics and Gynecology, Feinberg School of Medicine, Northwestern University, Chicago, IL, 60611, USA

## ARTICLE INFO

## Keywords:

follicular fluid  
Fallopian tube epithelium  
Ovarian cancer  
Vitronectin

## ABSTRACT

Ovarian cancer (OC) is deadly, and likely arises from the fallopian tube epithelium (FTE). Despite the association of OC with ovulation, OC typically presents in post-menopausal women who are no longer ovulating. The goal of this study was to understand how ovulation and aging interact to impact OC progression from the FTE. Follicular fluid released during ovulation induces DNA damage in the FTE, however, the role of aging on FTE exposure to follicular fluid is unexplored. Follicular fluid samples were collected from 14 women and its effects on FTE cells was assessed. Follicular fluid caused DNA damage and lipid oxidation in an age-dependent manner, but instead induced cell proliferation in a dose-dependent manner, independent of age in FTE cells. Follicular fluid regardless of age disrupted FTE spheroid formation and stimulated attachment and growth on ultra-low attachment plates. Proteomics analysis of the adhesion proteins in the follicular fluid samples identified vitronectin, a glycoprotein responsible for FTE cell attachment and spreading.

## 1. Introduction

High grade serous ovarian cancer (HGSOC) is the most lethal gynecological malignancy [1]. The identification of the fallopian tube epithelium (FTE) as a source of HGSOC has allowed researchers to study the stepwise progression of tumorigenesis, improve early detection, increase opportunistic salpingectomy procedures, and provide opportunities to impede tumor growth at the primary metastatic site [2–5]. There is a correlation between HGSOC and ovulation based on data from patients taking birth control pills or pregnant women that indicates that ovulation suppression reduces the risk of ovarian cancer [6]. Despite the association of ovarian cancer with ovulation, this disease typically presents as late stage metastatic cancer in post-menopausal women who are no longer ovulating [7–9]. Data derived from models suggests around a seven-year period between tumor initiation and clinical detection [10, 11]. Therefore, a major question in the field is how ovulation and aging contribute to HGSOC initiation in the FTE and its progression.

The FTE is regularly exposed to follicular fluid (FF) during ovulation, and recent literature has demonstrated that exposure to FF increases tumorigenic properties in the FTE cells. Exposure of FTE to FF upregulates expression of inflammatory cytokines such as

\* Corresponding author.

E-mail address: [joannab@uic.edu](mailto:joannab@uic.edu) (J.E. Burdette).

<sup>1</sup> Lead contact.

Interleukin-8 and DNA repair pathways, along with an increase in cell proliferation and accumulation of the tumor suppressor protein 53 (TP53) [12]. Expression of mutant p53 is common in fallopian tube precursor lesions and is considered a hallmark of HGSOE [13, 14]. Additional reports demonstrated that FF caused increased DNA damage in FTE cells [15]. FF induced intracellular reactive oxygen species (ROS) and DNA double strand breaks in the secretory cells of fimbriae epithelium [16]. Ovarian brain-derived neurotrophic factor in the FF was also shown to contribute to the progression of FTE lesions into widespread HGSOE [17]. FF promotes FTE cell migration, anchorage independent growth, cell invasion, peritoneum attachment, and cell proliferation via the Akt pathway [18].

In the ovary, FF contributes to the growth and quality of the oocyte, which is surrounded by this fluid. In terms of composition, FF is rich in lipids, hormones, large polysaccharides, growth factors and inflammatory cytokines [19]. Previously, it was demonstrated that FF becomes fibro-inflammatory with reproductive age. This study identified a unique cytokine profile (IL-3, IL-7, IL-15, TGF $\beta$ 1, TGF $\beta$ 3 and MIP-1) which showed direct correlation with chronologic age. Interestingly, this cytokine signature was independent of body mass index and showed inverse correlation with anti-Mullerian hormone levels [20]. Furthermore, the antioxidant capacity of FF is impaired with increased reproductive age leading to reduction in ROS scavenging efficiency [21].

In this study, we characterized the effect of human FF samples from reproductively young and old women on FTE cells. We found that FF induced DNA damage and lipid oxidation in an age-dependent manner in FTE cells. Further, FF increased cell proliferation in a dose-dependent manner, but not in an age dependent one. Interestingly, we found that FF abrogated FTE spheroid formation, stimulating disaggregation and promoting adhesion and spreading of FTE cells on ultra-low attachment (ULA) surfaces. Proteomic analysis identified vitronectin in FF responsible for mediating cell attachment and spreading on low attachment surfaces.

## 2. Results

### 2.1. Aged FF samples induce more DNA damage and lipid peroxidation compared to younger samples

Ovulation and aging are both risk factors for ovarian cancer, so we sought to determine if exposure to FF released during ovulation enhanced DNA damage and lipid peroxidation in FTE cells using samples taken from women of different ages. To test this hypothesis, we used FF samples from 14 women (7 reproductively young (29–35 years) and 7 reproductively aged (40–42 years)) undergoing assisted reproductive technology. Fig. 1A contains a summary of the FF samples used in this study. To determine if there was an age dependent effect on DNA damage induction in FTE cells, we treated FTE cells: FT190 (SV40 immortalized) and FT282 (pre-malignant model with p53<sup>R175H</sup> mutant) with FF samples (diluted 1:1 with serum-free culture media) from young (Y1–Y7) and aged (A1–A7) women and analyzed expression of the DNA damage marker  $\gamma$ H2.Ax by immunoblotting. Fig. 1B shows higher expression of  $\gamma$ H2.AX in FTE cells treated with aged FF samples compared to young FF samples in both cell lines tested. Fig. 1C displays the densitometric analysis, where each participant sample is a biological replicate, and we found a significant age-dependent difference of FF exposure in both cell lines tested.

To further determine how FF leads to DNA damage, we performed a lipid peroxidation assay which measures the degradation of lipids as a marker for oxidative stress. We observed significantly higher lipid degradation in FTE cells treated with aged FF samples

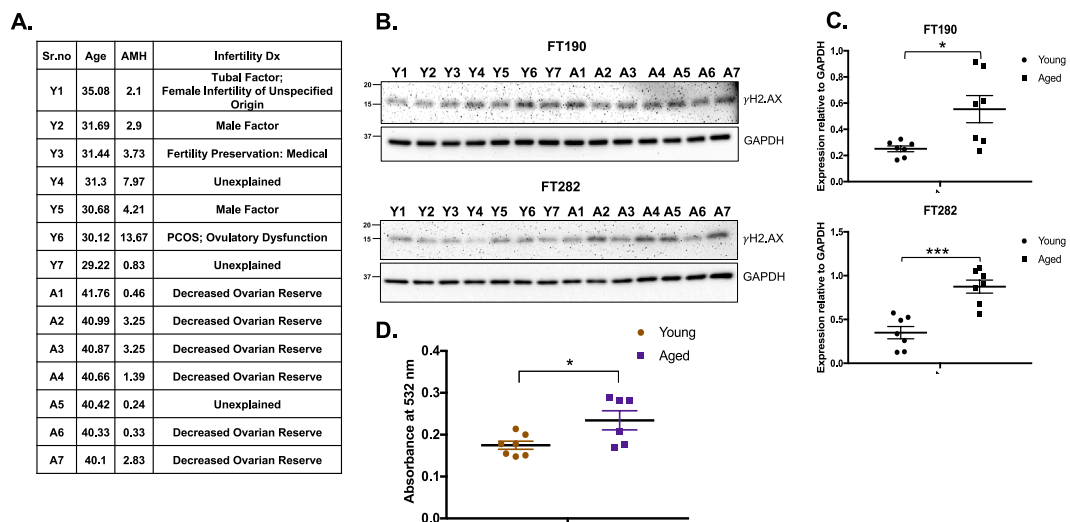


**Fig. 1.** Aged FF samples induce more DNA damage and lipid peroxidation compared to younger samples

A. Table summarizing young (Y1–Y7) and aged (A1–A7) FF samples with the age and cause of infertility used in this study. B. Representative immunoblot for  $\gamma$ H2.AX expression in FT190 and FT282 cells treated with FF samples (diluted 1:1 with serum-free culture media. Total volume = 2 ml) for 24 h. GAPDH was used as a loading control. C. Densitometry analysis for  $\gamma$ H2.AX expression in FT190 and FT282 cells treated with FF samples for 24 h. Normalization was performed relative to loading control GAPDH. D. Lipid peroxidation results of FT190 cells treated with young and aged FF samples for 24 h. Graph represents absorbance of MDA product measured colorimetrically at 532 nm.

relative to young FF samples (Fig. 1D).

## 2.2. Cell proliferation is increased in a dose dependent pattern by FF treatment in FTE cells

Several studies have shown that FF enhances cell proliferation in FTE cells as well as cancer cells [12,15,16,18]. To determine if there is an age dependent effect on cell proliferation, we treated FT190 and FT282 cells with FF samples and measured cell proliferation after 72 h by SRB assay. Although, FF significantly enhanced proliferation of FTE cells, we did not observe an age-dependent pattern in terms of cell proliferation. As shown in Fig. 2 A-B, FF treatment increased proliferation of FTE cells in a dose-dependent pattern with changes observed from the addition of 25 and 50% FF relative to serum free and serum containing media. Patient variability was observed based on the change of proliferation between the FF samples. Cyclin E1 expression drives proliferation and is frequently amplified in HGSOE [22]. Therefore, we investigated the effect of FF treatment on cyclin E1 expression. We found that FF increased cyclin E1 expression in a dose dependent pattern in FTE cells. (Fig. 2C–D).

## 2.3. FF abrogated FTE spheroid formation and enhanced adhesion to low attachment surfaces

FF has been shown to promote anchorage independent growth, anoikis resistance, cell invasion and peritoneum attachment [18]. Anoikis resistance is a unique property acquired by cancer cells to survive in the absence of attachment to the extracellular matrix (ECM) and is critical for primary metastasis of fallopian tube lesions [23]. Generating 3D spheroids is a simple, *in vitro* model system to study anoikis resistance and the early stages of tumorigenesis [24]. To determine if there was a difference in FTE cell spheroid formation when exposed to either young or aged FF samples, we seeded FT190 cells in a round bottom ULA plate to form 3D spheroids and treated the cells with FF samples for 3 days. Interestingly, FF treatment caused FT190 cells to migrate out of 3D spheroids, attach, and proliferate on ULA plates as a monolayer. FTE spheroid did not disintegrate completely after FF treatment. Untreated cells formed 3D spheroids (Fig. 3A) indicating that FBS did not allow for the cells to attach. This phenotype was specific for FT190 cells. FT194 and FT282 cells did not form spheroids. For OVCAR8 cells, we observed an increase in the spheroid size in presence of FF (Supplemental Fig. S1). FF mediated FTE cell adhesion was quantified by performing an SRB assay which showed higher absorbance due to enhanced cell attachment onto the ULA surface (Fig. 3B). We validated this finding with multiple FF samples and observed similar findings at an earlier and later timepoint (Day 5 and Day 15) of FF treatment. This effect was independent of age as both young and aged FF treatment caused attachment and proliferation of FT190 cells on the ULA surface (Fig. 3C).

We were interested in determining if FT190 cell attachment and proliferation on ULA plate was due to specific components in FF or if treatment with FF caused FTE cells to alter their signaling to encourage growth on the ULA surface. Therefore, we coated ULA plates with FF samples for different timepoints (4 h, 16 h, 24 h), washed away the non-adhered material, and then seeded FT190 cells. As shown in Fig. 3D–E, 4 hrs of FF coating is sufficient for FT190 cells to attach and proliferate on the FF coated ULA plates. We validated and quantified this finding by performing the SRB assay using 3 young and 3 aged FF samples. We coated ULA plates with FF samples

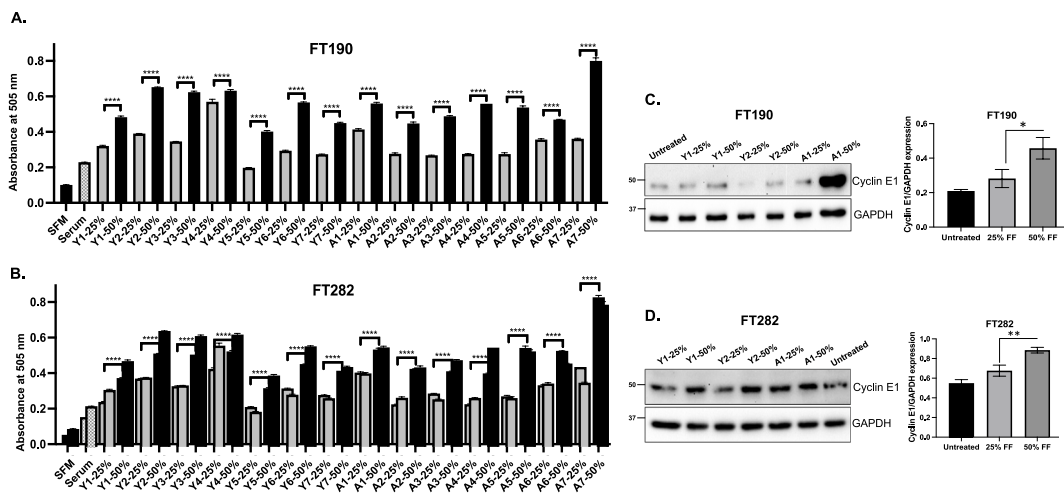


**Fig. 2.** Cell proliferation is increased in a dose dependent pattern by FF treatment in FTE cells

A. FT190 cells were treated with serum free media (SFM), serum containing media (serum) and FF samples diluted to 25% or 50% with SFM for 72 h. Cell proliferation was analyzed using an SRB assay. B. FT282 cells were treated with serum free media (SFM), serum containing media (serum) and FF samples diluted to 25% or 50% with SFM for 72 h. Cell proliferation was analyzed using an SRB assay. C. Representative immunoblot for cyclin E1 expression in FT190 cells treated with FF samples diluted to 25% or 50% with SFM for 48 h. GAPDH was used as a loading control. Bar graph represents densitometry analysis for cyclin E1 expression in FT190 cells treated with 25% and 50% FF samples for 24 h. Normalization was performed relative to loading control GAPDH. D. Representative immunoblot for cyclin E1 expression in FT282 cells treated with FF samples diluted to 25% or 50% with SFM for 48 h. GAPDH was used as a loading control. Bar graph represents densitometry analysis for cyclin E1 expression in FT282 cells treated with 25% and 50% FF samples for 24 h. Normalization was performed relative to loading control GAPDH.

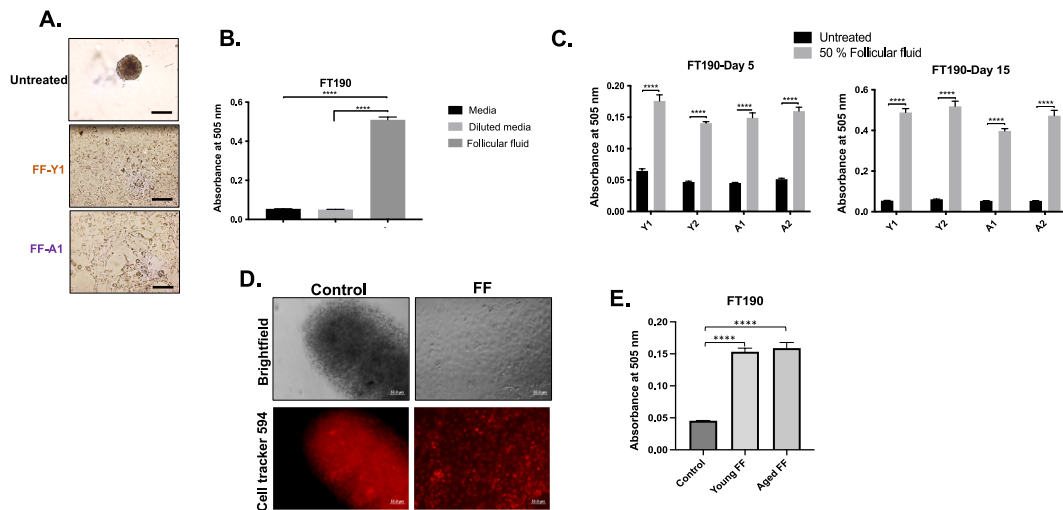


**Fig. 3.** FF abrogated FTE spheroid formation and enhanced adhesion to low attachment surfaces  
 A. Representative brightfield images of FT190 spheroids in a ULA plate treated with and without FF samples. 14 FF samples were tested. Images were captured at Day 3. Scale bar = 200  $\mu$ m. B. Cell proliferation was measured using an SRB assay at Day 3 of treating cells with and without FF samples. n = 14. Media refers to serum containing media and diluted media refers to media diluted 1:1 with serum-free media. C. Cell proliferation was measured using an SRB assay at Day 5 and Day 15 of treating cells with and without FF samples (Y1, Y2, A1, A2). Two random young (Y1, Y2) and two random aged (A1, A2) samples were used for treatment. FF samples were diluted 1:1 with serum-free media (i.e. 50% follicular fluid). n = 4. D. Representative brightfield and fluorescent images of FT190 cells seeded on a 6-well ULA plate coated with and without FF sample for 4 h. Wells were washed with 1X PBS and labelled FT190 cells (10, 000 cells/well) were seeded on the coated plates. Images were acquired after 24 h using a 10 $\times$  objective of fluorescent microscope. Scale bar = 50  $\mu$ m. E. Cell proliferation was measured using an SRB assay to measure cell viability of FT190 cells on FF (young (Y1, Y2, Y3) and aged (A1, A2, A3) samples, n = 3) coated ULA plates.

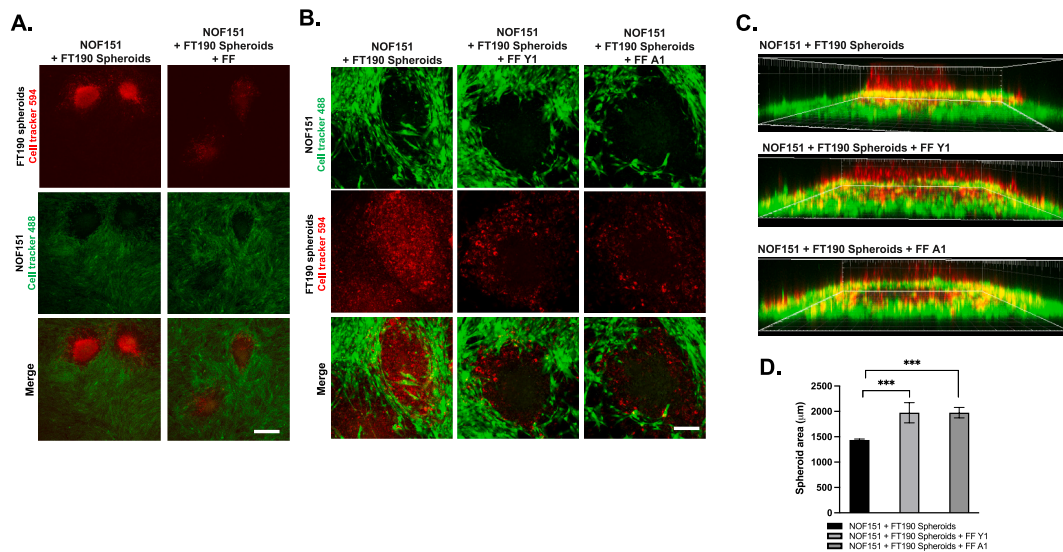


**Fig. 4.** FF contributes to FTE spheroid disaggregation and spreading onto ovarian fibroblasts  
 A. Representative images acquired by fluorescence microscopy of FT190 spheroids (labelled with Cell tracker 594) on NOF151 cells (labelled with Cell tracker 488) with and without FF (24 h). Scale bar = 100  $\mu$ m. B. Representative Z stack images (maximum intensity projection) acquired by confocal microscopy of FT190 spheroids (labelled with Cell tracker 594) on NOF151 cells (labelled with Cell tracker 488) with and without young and aged FF samples (24 h). Scale bar = 200  $\mu$ m. C. A maximum intensity projection re-construction of a three-dimensional FTE spheroid (labelled with Cell tracker 594) optical data stack over the surface of NOF151 cells (labelled with Cell tracker 488) treated with young (Y1) and aged (A1) FF samples. Spheroids were imaged with a 10 $\times$  objective and re-constructed using the Imaris software. D. Spheroid area (with and without FF) was determined by quantification of red fluorescent intensity using a polygon area measurement tool of the Imaris software.

for 4 h before seeding the cells and found increased viability of the cells (Fig. 3E). This suggested that FF contains factors that can coat the ULA surface and promote FTE cells attachment. Interestingly, coating low attachment surface with FF allowed attachment and proliferation of FTE cells (FT190, FT194, FT282) as well as ovarian cancer cells (OVCAR4 and OVCAR8) independent of age (Supplemental Fig. S2).

#### 2.4. FF contributes to FTE spheroid disaggregation and spreading onto ovarian fibroblasts

In recent years, several hypotheses regarding the steps involved between ovarian cancer initiation in the FTE and dissemination to the ovary and peritoneal cavity have been presented. One of the most popular hypotheses, which is the 'seeding hypothesis,' suggests that precursor FTE cells acquire oncogenic properties and are able to attach and invade through the ovarian stroma [9]. Hence, to determine if FF aids FTE cells in attachment and/or invasion through the ovarian stroma, we performed a co-culture experiment. Here, we used ovarian fibroblast cells NOF151 to mimic the ovarian stroma. We generated FT190 spheroids using ULA plates and added the spheroids onto a monolayer of NOF151 cells with and without FF. NOF151 cells and FT190 spheroids were labelled with fluorescent cell tracker dyes to distinguish the two cell types under the microscope. In the absence of FF, the spheroids are brightly fluorescent, and images depicted a more compact arrangement. However, in the presence of the FF, FT190 spheroids showed significantly reduced fluorescence relative to the untreated control (Fig. 4A). Imaging of spheroids via confocal microscopy to obtain a three-dimensional picture revealed reduced red fluorescence and enhanced FTE cell spreading in the FF treated samples (Fig. 4B-C). FTE cell spreading was quantified by measuring the red fluorescence after drawing a polygon around the spheroids using the Imaris software. As shown in Fig. 4D, FF enhanced FTE cell spreading on the surface of NOF151 cells independent of age.

#### 2.5. Proteomic analysis of FF samples revealed extracellular matrix (ECM) protein - vitronectin as the component responsible for FTE adhesion and spreading

Since our data suggests that FF promotes attachment and proliferation of the FTE cells to ULA surface and ovarian fibroblasts, we sought to identify FF factors responsible for this phenotype using proteomics. Several studies have characterized the proteins in FF. However, we were interested in identifying the crucial components required for attachment and proliferation of FTE on a ULA surface. Hence, we coated ULA plates with 3 young and 3 aged FF samples for 4 h, washed off the excess FF and added lysis buffer to the plate for proteomic identification (workflow shown in Fig. 5A). Mass spectrometry analysis revealed 31 and 19 proteins in young and aged FF samples respectively. Interestingly, vitronectin was the only protein present in all 6 FF samples (3 young and 3 aged) belonging to the ECM pathway (Fig. 5B). We confirmed this finding by performing immunoblotting of FF samples (Fig. 5C). Different concentrations of recombinant vitronectin protein were utilized to determine the concentration of FF vitronectin via quantitative Western blot. As shown in Fig. 5C, the vitronectin content in FF samples was found to be  $\sim 0.1 \mu\text{g}/\mu\text{l}$ .

We wanted to validate whether purified vitronectin caused a similar phenotype as FF in terms of cell adhesion, spreading and proliferation on ULA surface. Hence, we performed a cell adhesion assay by coating ULA plates for 4 h with FF and recombinant vitronectin (1  $\mu\text{g}$ ) and seeded FT190 cells. As shown in Fig. 6A, vitronectin promotes cell adhesion and proliferation similar to FF. Cells seeded on uncoated ULA surfaces formed cellular aggregates. We validated this finding by performing the SRB assay at 48 h to demonstrate that the cells are viable and proliferating (Fig. 6B). Coating low attachment surface with vitronectin (1  $\mu\text{g}$ ) for 4 h allowed attachment and proliferation of FTE cells (FT190, FT194, FT282) as well as ovarian cancer cells (OVCAR4 and OVCAR8)

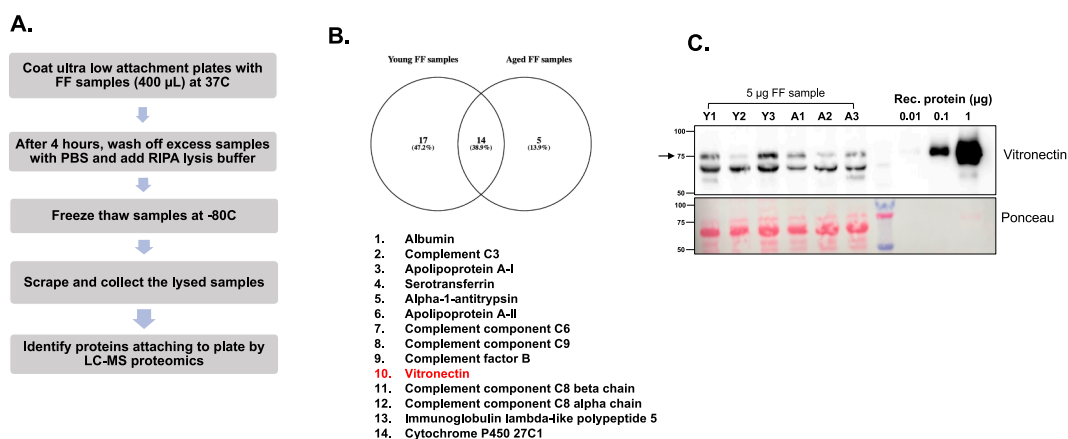


**Fig. 5.** Proteomic analysis of FF samples revealed extracellular matrix (ECM) protein - vitronectin as the component responsible for FTE adhesion and spreading

A. Experimental workflow of proteomics experiment. B. Venn diagram showing 14 common proteins identified between young and aged FF samples from proteomics analysis. Common proteins are listed with vitronectin (highlighted in red). C. Representative immunoblot for vitronectin expression in 3 young (Y1-Y3) and 3 aged (A1-A3) FF samples. FF samples (5  $\mu\text{g}$ ) and recombinant vitronectin protein (0.01  $\mu\text{g}$ , 0.1  $\mu\text{g}$ , 1  $\mu\text{g}$ ) diluted with lysis buffer were used for immunoblotting. Arrow represents the band analyzed for vitronectin. Ponceau staining was used for loading control.

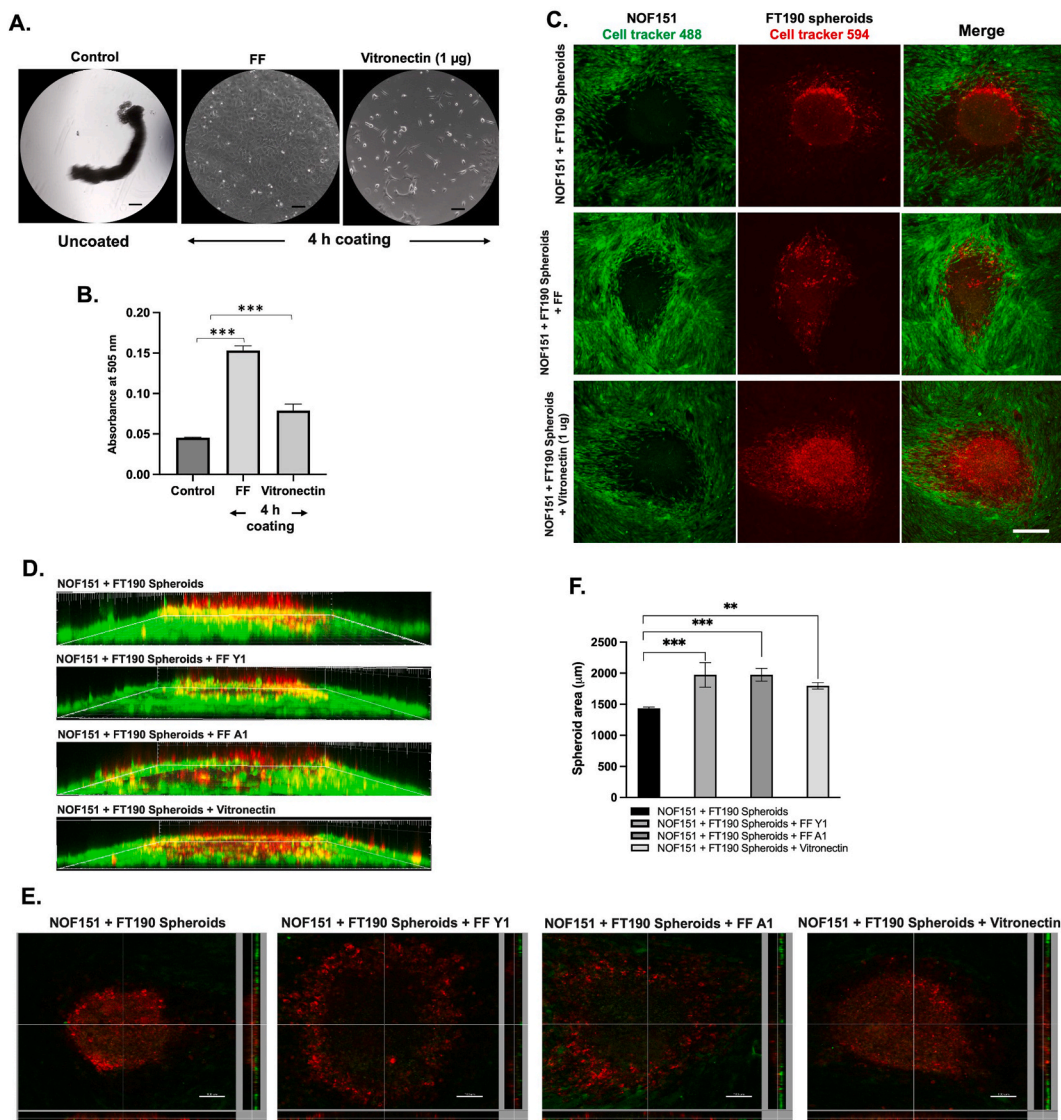


**Fig. 6.** Vitronectin in FF aids in FTE adhesion and spreading

A. Representative brightfield images of FT190 cells seeded on ULA plates coated with FF sample (400  $\mu$ l) and recombinant vitronectin protein (1  $\mu$ g/well) for 4 h. Wells were washed with 1X PBS and FT190 cells were seeded on the coated plates. Images were acquired after 24 h. Scale bar = 200  $\mu$ m. B. Cell proliferation was measured using an SRB assay to measure cell viability of FT190 cells on FF and vitronectin coated ULA plates. C. Representative Z stack images acquired by confocal microscopy of FT190 spheroids (labelled with Cell tracker 594) on NOF151 cells (labelled with Cell tracker 488) with FF samples and recombinant vitronectin protein (1  $\mu$ g) (24 h). Scale bar = 200  $\mu$ m. D. A maximum intensity projection reconstruction of a three-dimensional FTE spheroid (labelled with Cell tracker 594) optical data stack over the surface of NOF151 cells (labelled with Cell tracker 488) treated with FF samples (Y1, A1) and vitronectin (1  $\mu$ g). Spheroids were imaged with a 10 $\times$  objective and re-constructed using the Imaris software. E. Representative images acquired by confocal microscopy showing a side and top projection of the FT190 spheroids on NOF151 cells with FF samples and recombinant vitronectin protein (1  $\mu$ g) (24 h). Scale bar = 100  $\mu$ m. F. Spheroid area (with and without FF/vitronectin) was determined by quantification of red fluorescent intensity using a polygon area measurement tool of the Imaris software.

(Supplemental Fig. S3).

Further, we performed a co-culture assay to determine if vitronectin facilitates cell migration and proliferation on ovarian fibroblasts. We generated FT190 spheroids and seeded them on a monolayer of NOF151 cells. Then, the cells were treated with media, FF (100%) and vitronectin (1  $\mu$ g/well). Images were acquired after 24 h using a confocal microscope. Both vitronectin and FF enhanced FT190 cell spreading over NOF151 cells (Fig. 6C–D). Spheroid thickness, depth of spheroid attachment and, spreading was visualized by constructing FT190 spheroid optical data showing a side projection of the FTE spheroids (Fig. 6D–E). Area of spheroids (red fluorescence) was quantified as shown in Fig. 6F.

### 3. Discussion

Despite ovarian cancer typically being detected in post-menopausal women, ovulation is a major risk factor for HGSOE [7–9]. Thus, our study attempts to determine whether age-dependent changes in FF enhance progression of FTE derived HGSOE. The FTE is regularly exposed to FF during ovulation and the cytokine composition of FF becomes more fibro-inflammatory with age [20]. Although it is well-established that aging reduces the quality of the oocyte which is surrounded by FF, the role of FF on FTE and its ability to drive carcinogenesis with age is under-studied.

FF increased proliferation, migration, and anchorage independent growth in FTE cells [12,15,16]. Our data showed that FF augments  $\gamma$ H2AX expression in non-transformed immortal FTE as well as premalignant cell models. Further, the DNA damage response pathway activation occurs in an age-dependent manner, as we show a significant difference between FTE cells treated with the young and aged FF samples. Lipid peroxidation is an indicator of oxidative stress, and our data showed that aged FF samples caused higher lipid peroxidation relative to young samples. This finding is supported by recent studies demonstrating that FF becomes more inflammatory with age [20]. Interestingly, the antioxidant capacity of FF is impaired in older women, and there is age-dependent difference in the metabolomics profiles of FF in terms of hormones, lipid oxidation enzymes, microRNAs etc [21]. Consistent with recent studies, our study reveals that FF increases the proliferation of FTE cells; however, we do not find an age-dependent effect in enhancing cell proliferation. Proliferation was increased in a dose-dependent pattern which was validated by enhanced expression of cyclin E1, a protein important for cell cycle G1/S transition. Importantly, in terms of ovarian cancer, cyclin E1 amplification occurs in about 40% of tumors and is reported in the early stages of tumorigenesis [22].

FF promoted attachment of FT190 cells on a ULA surface and allowed the cells to disassociate from the 3D spheroids onto the ULA surface. We collected proteins deposited on the ULA surface to determine the molecular mechanism by which FF led to FTE cell adhesion. These data suggested that FF has a potential role in attachment of premalignant FTE cells to ovarian stroma and ECM during metastasis. We identified vitronectin, an adhesive glycoprotein in all the 6 FF samples subjected to proteomics as a potential driver in this process. The presence and amount of vitronectin was the same regardless of the age of the FF samples, which was consistent with our *in vitro* findings that all the FF samples tested caused FTE adhesion on ULA surfaces. Vitronectin is a secreted glycoprotein with a well-established role in cell adhesion and migration by linking cells to the ECM via integrins, urokinase plasminogen activator receptor and plasminogen activator inhibitor-1 [25]. Studies in bovine model have shown that vitronectin in FF contributes to follicle development [26]. Additionally, vitronectin promotes sperm-oocyte linking and fertilization [27–29].

Vitronectin was the only ECM protein identified in our proteomics experiment across all FF samples which would indicate a role in ULA surface attachment further suggesting a role in FTE cell adhesion. Both FF and vitronectin allowed FTE cells to disassociate from the spheroids and colonize a monolayer of ovarian fibroblasts. However, vitronectin mediated FTE and HGSOE cell attachment and spreading was not equivalent to FF indicating additional factor/s in FF which along with vitronectin facilitate cell spreading and possibly invasion through ovarian stromal cells based on the use of NOF cells as a model system. In ovarian cancer, vitronectin is crucial for MMP-2 mediated attachment of tumor cells to the peritoneum and omentum [30,31]. This is the first study to identify vitronectin in FF and its ability to modify FTE cells thereby encouraging their adhesion and survival on ultralow surfaces and ovarian stromal cells. To the best of our knowledge, there are no commercially available inhibitors against vitronectin, hence we confirmed our findings using recombinant vitronectin protein.

Although exposure to FF increases cell proliferation, oxidative stress and DNA damage, an age-dependence has never been examined. Aging is associated with ovarian fibrosis and ovarian cancer cells favor a collagen-rich matrix for adhesion and expansion [32,33]. Since vitronectin was not associated with age-dependent changes in stromal adhesion and spreading, it is likely that the aging ovarian microenvironment and aspects of fibrosis contribute to age associated HGSOE spread. Overall, our data show that age-related changes in FF contributes to increased DNA damage and lipid peroxidation in the FTE. Further, we identified vitronectin in FF to promote attachment and growth of FTE cells indicating a potential role in attachment of precursor cells to ovarian stroma during metastasis.

### 4. Limitations of the study

Despite these findings, the current study has certain limitations. Future studies will focus on prolonged or repeated exposure of FF to FTE cells or from a wider range of biological ages. The underlying reason that a patient seeks IVF could impact the follicular fluid composition and thus could impact the changes in the fallopian tube in an age-independent manner. Since we observed enhanced lipid peroxidation and DNA damage in aged FF samples, it will be interesting to determine if there is an age-dependent change in DNA damage repair pathways. Future studies treating primary fallopian tube tissue would also complement the cell model system.

### Financial Support

NIH CA240423, NIH CA240301.

### Ethics statement

FF samples were collected from women undergoing assisted reproductive technology through the Northwestern University Reproductive Tissue Library (NU-RTL), under an Institutional Review Board - approved tissue repository protocol (# STU00072811), following written informed consent from all participants involved in the study. The study complies with all the regulations approved by

the protocol.

## STAR methods

### Compounds

Recombinant human vitronectin (R&D systems#2308-VN-050) was resuspended in dimethyl sulfoxide (DMSO) with final DMSO concentration <0.1% (v/v).

### FF samples

FF samples were collected as described [20]. Briefly, de-identified FF samples were collected from 14 women (7 reproductively young and 7 reproductively aged) undergoing assisted reproductive technology through the Northwestern University Reproductive Tissue Library under an IRB approved protocol, following written informed consent. Information regarding the FF samples is summarized in Fig. 1A. Samples were aliquoted and stored at  $-80^{\circ}\text{C}$  until further use. Each aliquot was thawed for a maximum of two times before experiments. Bradford was used to determine protein concentration of FF samples.

### Cell culture

Immortalized fallopian tube secretory cells (FT190, FT194, FT282) were a gift from Ronny Drapkin (University of Pennsylvania) and were cultured using  $\alpha$ -MEM-Cellgro media (Corning #10-022-CV) as described [34]. OVCAR-8 cells were obtained from NCI Cell Bank. and grown in DMEM with 10% FBS (Fetal Bovine Serum GeminiBio#100-106) and 1% P/S (Penicillin-Streptomycin Fisher#15070063). Ovarian fibroblast cell line (NOF) immortalized with p53 siRNA and hTERT called NOF151 was a gift from Jinsong Liu [35]. These cells were maintained in Medium 199 and MCDB105 medium (1:1) supplemented with 10% FBS, 1% P/S and 5  $\mu\text{g}$  EGF. Cells were passaged <20 times and maintained in a humidified incubator at  $37^{\circ}\text{C}$  in 5%  $\text{CO}_2$  environment. Experiments were performed with mycoplasma free cells and all cell lines have been authenticated using STR profiling <3 years.

### Liquid chromatography-mass spectrometry (LC-MS) sample preparation and data analysis

ULA plates were coated with FF samples (400  $\mu\text{L}$ /well) for 4 h at  $37^{\circ}\text{C}$  in a 5%  $\text{CO}_2$  environment. Excess samples were washed off with 1X PBS. Samples were collected in 100  $\mu\text{L}$  of RIPA buffer [50 mM Tris pH 7.6, 150 mM NaCl, 1% Triton X-100, 0.1% SDS with protease and phosphatase inhibitors] then freeze thaw at  $-80^{\circ}\text{C}$ . In solution digestion of proteins was performed with 4 M urea and 100 mM TEAB. Proteins were reduced by 10 mM of dithiothreitol for 30 min at room temperature, followed by alkylation with 30 mM iodoacetamide at room temperature in the dark for 30 min. Samples were digested overnight with trypsin ( $37^{\circ}\text{C}$ ). Strong cation exchange was carried out, and the eluate was desalted using C18 Zip-Tip. The peptides were dried in a Speed-vac and resuspended in 15  $\mu\text{L}$  of 0.1 % formic acid.

Each sample was injected onto the Agilent 1260 Infinity nanoLC system and analyzed with the Thermo Q-Exactive mass spectrometer. Peptides were loaded onto an Acclaim PepMap 100 trap column (75  $\mu\text{m} \times 2$  cm nanoViper, C18, 3  $\mu\text{m}$  100  $\text{\AA}$ ) with 0.1 % formic acid (flowrate = 2  $\mu\text{L}$ /min). The peptides were separated with flowing rate at 0.25  $\mu\text{L}$ /min on an Agilent Zorbax 300SB-C18 column (0.075  $\times$  150 mm, 3.5  $\mu\text{m}$  300  $\text{\AA}$ ) using a 60-min gradient, from 5% of 0.1% formic acid in acetonitrile to 30% over 60 min. Spraying voltage on the mass spectrometer was set to 1.6 kV and the capillary temperature at  $250^{\circ}\text{C}$ . Data was collected in the data-dependent analysis mode at a mass resolution of 70,000 and scan range 375–2000  $m/z$ . Automatic gain control target was  $1 \times 10^6$  for a maximum injection time 100 ms. For MS/MS analysis, the top 10 most abundant precursors within a charge state range of 2–5 were selected. MS/MS spectra were acquired at a resolution of 17,500, AGC target at  $1 \times 10^5$ , and maximum IT of 50 ms. All raw mass spectrometry data is publicly available on MassIVE (project ID MSV000092269).

The raw MS data was imported to the Thermo Proteome Discoverer Software for protein identification against the curated Swiss-Prot *Homo Sapiens* database. The precursor mass tolerance was set to 10 ppm. Database searching was employed with Sequest HT search engine, and peptides mass range was set from 350 to 6500 Da, containing 6 to 144 amino acids, with  $\leq 2$  missed cleavages. Fragment masses were searched with a tolerance of  $\pm 0.02$  Da. Dynamic modifications included were oxidation (+15.995 Da; M) and acetylation (+42.011 Da; N-terminus). The static modification included was carbamidomethylation (+57.021 Da; C). Minimum of one unique peptide were used for identification. Venn diagram to depict common proteins across samples was generated using Venny [36].

### Lipid peroxidation assay

Oxidative damage was determined using Lipid peroxidation assay kit (Sigma MAK085) as per manufacturer's instructions. Briefly, FT190 cells (10,000 cells/well) were seeded in a 6-well plate and treated with FF samples for 24 h (diluted 1:1 with serum-free culture media. Total volume = 2 ml). FF-induced lipid oxidation was measured by colorimetric quantification (532 nm) of end-product malondialdehyde using Synergy BioTek plate reader.

### Immunoblot analysis

Cells were lysed in RIPA buffer and immunoblot analysis was performed as described [37]. Membranes were incubated with primary antibody (Table 1) overnight at 4 °C following incubation with secondary antibody (Table 2) prior to visualization of signal with SuperSignal™ West Femto substrate (Thermo Fisher) and imaging on a FluorChem E system (ProteinSimple).

### Cell proliferation assay

Cell proliferation was measured by a sulforhodamine B (SRB) assay as described [38]. Cells were seeded in 96-well, clear, flat-bottomed plate at 3000 cells/well and allowed to attach overnight. Cells were treated with FF samples (100 µL/well) and proliferation rate was quantified by measuring absorbance (505 nm) after 72 h of treatment on a Synergy BioTek plate reader. Complete media and serum free media were used as control treatment and absorbance values were normalized to blank wells.

### Generation of 3D spheroids

5000 cells (FT190, FT194, FT282, OVCAR8) were resuspended in 100 µL of their respective media/well in 96-well round bottom ULA plate (Corning 07-201-680) and allowed to form spheroids for 14 days. For treatment with FF, spheroids were generated by suspending 5000 cells in 50 µL of media/well in the ULA Plate and treated with 50 µL of FF after 24 h of seeding. For proliferation assay, cells were allowed to form spheroids for 3, 5 or 15 days as described in the figure legends.

### Cell spreading assay

24-well ULA plates were coated with FF or vitronectin for 4 h. FT190 cells were labelled with CellTracker™Red CMTPX dye as per manufacturer's instructions. Wells were washed with 1X PBS and cells were seeded at 3000 cells/well. Images were acquired after 24 h using 4X/10× objective (594 nm) on a Nikon Eclipse E600 microscope using DS-Ri1 digital camera and NIS Elements Software (Nikon Instruments).

### Confocal microscopy

FT190 spheroids were generated using ULA plates (Corning 07-201-680) over a period of 2 weeks. Spheroids were labelled with CellTracker™Red CMTPX dye and NOF151 cells were labelled with CellTracker™Green CMFDA Dye as per manufacturer's instructions. NOF151 cells (3000 cells/well) were seeded in glass bottom chamber slides (Ibidi #80427) to reach 100% confluence overnight. Labelled FT190 spheroids were added on the NOF151 monolayer such that every well contains 10 spheroids. Media/FF/vitronectin (total volume 300 µL/well) were added to the cells as per the treatment condition and incubated for 24 h. Cells were fixed using 4% paraformaldehyde and images were acquired using 10× objective on a Zeiss LSM 710 confocal microscope. Image analysis was performed using Imaris 7.7 software.

### Statistical analysis

Data presented are the mean ± standard error of the mean and represent at least 3 independent experiments. Statistical analysis was carried out using GraphPad Prism software. For the *in vitro* cell line experiments, two-sample t-tests were used for two groups and One-way ANOVA was used to compare significance to the control. Adjusted  $p < 0.05$  is considered significant with stars denoting significance as follows: \* $p < 0.05$ , \*\* $p < 0.01$ , \*\*\* $p < 0.001$ , and \*\*\*\* $p < 0.0001$ .

### Data availability statement

The datasets generated during and/or analyzed during the current study are available from the corresponding author on reasonable request.

### CRedit authorship contribution statement

**Amrita Salvi:** Writing – review & editing, Writing – original draft, Investigation, Formal analysis, Data curation. **Wenping Li:** Formal analysis, Data curation. **Shweta S. Dipali:** Writing – review & editing, Resources. **Stephanie M. Cologna:** Writing – review & editing, Conceptualization. **Mary Ellen Pavone:** Resources. **Francesca E. Duncan:** Writing – review & editing, Conceptualization. **Joanna E. Burdette:** Writing – review & editing, Writing – original draft, Supervision, Funding acquisition, Conceptualization.

### Declaration of competing interest

The authors declare the following financial interests/personal relationships which may be considered as potential competing interests:

Joanna Burdette reports financial support was provided by National Institutes of Health. If there are other authors, they declare that

**Table 1**  
Primary antibodies.

Antibody	Source	Dilution for WB
Anti-rabbit $\gamma$ H2.AX	CST #9718	1:1000
Anti-rabbit GAPDH	CST #2118	1:10000
Anti-rabbit cyclin E1	CST #20808	1:1000
Anti-rabbit vitronectin	Proteintech 15833-1-AP	1:1000

**Table 2**  
Secondary antibodies and fluorophores.

Antibody	Source	Dilution for WB	Dilution for immunofluorescence
Anti-rabbit IgG-HRP	CST #7074	1:10000	–
CellTracker™Green CMFDA Dye	Invitrogen C7025	–	1:1000
CellTracker™Red CMTPX Dye	Invitrogen C34552	–	1:1000

they have no known competing financial interests or personal relationships that could have appeared to influence the work reported in this paper.

## Acknowledgement

The authors gratefully acknowledge the University of Illinois Chicago Research Resources Center's Fluorescence Imaging Core (FIC) for their guidance with acquiring and analyzing images on the confocal microscope. We acknowledge NIH CA240301 (JEB), CA240423 (JEB), OCRA Ann and Sol Schreiber Mentored Investigator award (AS), R01 CA240423 (SMC), R01 NS114413 (SMC), and Together Strong NPC Foundation (WL).

## Appendix A. Supplementary data

Supplementary data to this article can be found online at <https://doi.org/10.1016/j.heliyon.2024.e27336>.

## References

- [1] D.D.L. Bowtell, The genesis and evolution of high-grade serous ovarian cancer, *Nature Publishing Group* 10 (2010) 803–808.
- [2] A.L. Gross, R.J. Kurman, R. Vang, I.-M. Shih, K. Visvanathan, Precursor lesions of high-grade serous ovarian carcinoma: morphological and molecular characteristics, *Journal of Oncology* 2010 (2010) 126295–126299.
- [3] C.P. Crum, et al., The distal fallopian tube: a new model for pelvic serous carcinogenesis, *Curr. Opin. Obstet. Gynecol.* 19 (2007) 3–9.
- [4] S.M. King, J.E. Burdette, Evaluating the progenitor cells of ovarian cancer: analysis of current animal models, *BMB Rep* 44 (2011) 435–445.
- [5] A.M. Karst, K. Levanon, R. Drapkin, Modeling high-grade serous ovarian carcinogenesis from the fallopian tube, *Proc. Natl. Acad. Sci. USA* 108 (2011) 7547–7552.
- [6] T. Karlsson, T. Johansson, J. Höglund, W.E. Ek, Å. Johansson, Time-dependent effects of oral contraceptive use on breast, ovarian, and endometrial cancers, *Cancer Res.* 81 (2021) 1153–1162.
- [7] M.F. Fathalla, Incessant ovulation and ovarian cancer - a hypothesis re-visited, *Facts Views Vis Obgyn* 5 (2013) 292–297.
- [8] S.M. King, et al., The impact of ovulation on fallopian tube epithelial cells: evaluating three hypotheses connecting ovulation and serous ovarian cancer, *Endocr. Relat. Cancer* 18 (2011) 627–642.
- [9] M.M. Emori, R. Drapkin, The hormonal composition of follicular fluid and its implications for ovarian cancer pathogenesis, *Reprod. Biol. Endocrinol.* 12 (2014) 60.
- [10] S.I. Labidi-Galy, et al., High grade serous ovarian carcinomas originate in the fallopian tube, *Nat. Commun.* 8 (2017) 1093.
- [11] S. Kyo, N. Ishikawa, K. Nakamura, K. Nakayama, The fallopian tube as origin of ovarian cancer: change of diagnostic and preventive strategies, *Cancer Med.* 9 (2020) 421–431.
- [12] K. Bahar-Shany, et al., Exposure of fallopian tube epithelium to follicular fluid mimics carcinogenic changes in precursor lesions of serous papillary carcinoma, *Gynecol. Oncol.* 132 (2014) 322–327.
- [13] M. Tuna, et al., Clinical relevance of TP53 hotspot mutations in high-grade serous ovarian cancers, *Br. J. Cancer* 122 (2020) 405–412.
- [14] E. Kuhn, et al., TP53 mutations in serous tubal intraepithelial carcinoma and concurrent pelvic high-grade serous carcinoma-evidence supporting the clonal relationship of the two lesions, *J. Pathol.* 226 (2011) 421–426.
- [15] P. Brachova, N.S. Alvarez, B.J. Van Voorhis, L.K. Christenson, Cytidine deaminase Apobec3a induction in fallopian epithelium after exposure to follicular fluid, *Gynecol. Oncol.* 145 (2017) 577–583.
- [16] H.-S. Huang, et al., Mutagenic, surviving and tumorigenic effects of follicular fluid in the context of p53 loss: initiation of fimbria carcinogenesis, *Carcinogenesis* 36 (2015) 1419–1428.
- [17] M. Kang, et al., Ovarian BDNF promotes survival, migration, and attachment of tumor precursors originated from p53 mutant fallopian tube epithelial cells, *Oncogenesis* 9 (2020) 55.
- [18] C.-F. Hsu, P.-C. Chen, V. Seenan, D.-C. Ding, T.-Y. Chu, Ovulatory follicular fluid facilitates the full transformation process for the development of high-grade serous carcinoma, *Cancers* 13 (2021) 468.
- [19] R.J. Rodgers, H.F. Irving-Rodgers, Formation of the ovarian follicular antrum and follicular fluid, *Biol. Reprod.* 82 (2010) 1021–1029.
- [20] J.H. Machlin, et al., Fibroinflammatory signatures increase with age in the human ovary and follicular fluid, *Int. J. Mol. Sci.* 22 (2021) 4902.
- [21] H. Debbarh, et al., Antioxidant activities and lipid peroxidation status in human follicular fluid: age-dependent change, *Zygote* 29 (2021) 490–494.

- [22] A.M. Karst, et al., Cyclin E1 deregulation occurs early in secretory cell transformation to promote formation of fallopian tube derived high-grade serous ovarian cancers, *Cancer Res.* 74 (2014) 1141–1152.
- [23] Y.-N. Kim, K.H. Koo, J.Y. Sung, U.-J. Yun, H. Kim, Anoikis resistance: an essential prerequisite for tumor metastasis, *Int J Cell Biol* 2012 (2012) 306879.
- [24] L. Carduner, et al., Cell cycle arrest or survival signaling through  $\alpha v$  integrins, activation of PKC and ERK1/2 lead to anoikis resistance of ovarian cancer spheroids, *Exp. Cell Res.* 320 (2014) 329–342.
- [25] A. Bera, et al., Functional role of vitronectin in breast cancer, *PLoS One* 15 (2020) e0242141.
- [26] A.T. Peter, M.S. Perrone, E.K. Asem, Bovine ovarian follicular fluid vitronectin content is influenced by the follicle size, *Theriogenology* 43 (1995) 1239–1247.
- [27] F.M. Fusi, N. Bernocchi, A. Ferrari, R.A. Bronson, Is vitronectin the velcro that binds the gametes together? *Mol. Hum. Reprod.* 2 (1996) 859–866.
- [28] C.C. Boissonnas, et al., Role of sperm  $\alpha v$  integrin in mouse fertilization, *Dev Dyn* 239 (2010) 773–783.
- [29] V.M. Paes, J.R. de Figueiredo, P.L. Ryan, S.T. Willard, J.M. Feugang, Comparative analysis of porcine follicular fluid proteomes of small and large ovarian follicles, *Biology* 9 (2020) 101.
- [30] S. Kaur, et al.,  $\beta 3$ -Integrin expression on tumor cells inhibits tumor progression, reduces metastasis, and is associated with a favorable prognosis in patients with ovarian cancer, *Am. J. Pathol.* 175 (2009) 2184–2196.
- [31] H.A. Kenny, S. Kaur, L.M. Coussens, E. Lengyel, The initial steps of ovarian cancer cell metastasis are mediated by MMP-2 cleavage of vitronectin and fibronectin, *J. Clin. Invest.* 118 (2008) 1367–1379.
- [32] S.M. Briley, et al., Reproductive age-associated fibrosis in the stroma of the mammalian ovary, *Reproduction* 152 (2016) 245–260.
- [33] M. Dean, V. Jin, A. Russo, D.D. Lantvit, J.E. Burdette, Exposure of the extracellular matrix and colonization of the ovary in metastasis of fallopian-tube-derived cancer, *Carcinogenesis* 40 (2019) 41–51.
- [34] M. Dean, D.A. Davis, J.E. Burdette, Activin A stimulates migration of the fallopian tube epithelium, an origin of high-grade serous ovarian cancer, through non-canonical signaling, *Cancer Lett.* 391 (2017) 114–124.
- [35] A.S. Nagaraja, et al., Adrenergic-mediated increases in *INHBA* drive CAF phenotype and collagens, *JCI Insight* 6 (2021).
- [36] J.C. Oliveros, Venny. **An Interactive Tool for Comparing Lists with Venn's Diagrams, References - Scientific Research Publishing, 2007-2015.** [https://www.scirp.org/\(S\(lz5mqp453ed%20snp55rrgict55\)\)/reference/referencespapers.aspx?referenceid=2904043](https://www.scirp.org/(S(lz5mqp453ed%20snp55rrgict55))/reference/referencespapers.aspx?referenceid=2904043).
- [37] A. Salvi, et al., Verticillin A causes apoptosis and reduces tumor burden in high-grade serous ovarian cancer by inducing DNA damage, *Mol Cancer Ther* 19 (2020) 89–100.
- [38] V. Vichai, K. Kirtikara, Sulforhodamine B colorimetric assay for cytotoxicity screening, *Nat. Protoc.* 1 (2006) 1112–1116.